Appl Phys A (2014) 115:353–358
DOI 10.1007/s00339-013-7835-8

Applied Physics A
Materials Science & Processing

Structural and optical properties of glancing angle deposited In_2O_3 columnar arrays and Si/In_2O_3 photodetector

A. Mondal · B. Shougaijam · T. Goswami · J.C. Dhar · N.K. Singh · S. Choudhury · K.K. Chattopadhay

Received: 16 May 2013 / Accepted: 26 June 2013 / Published online: 25 July 2013
© Springer-Verlag Berlin Heidelberg 2013

Abstract Ordered and perpendicular columnar arrays of In_2O_3 were synthesized on conducting ITO electrode by a simple glancing angle deposition (GLAD) technique. The as-deposited In_2O_3 columns were investigated by field emission gun-scanning electron microscope (FEG-SEM). The average length and diameter of the columns were estimated ∼400 nm and ∼100 nm, respectively. The morphology of the structure was examined by transmission electron microscopy (TEM). X-ray diffraction (XRD) analysis shows the polycrystalline nature of the sample which was verified by selective area electron diffraction (SAED) analysis. The growth mechanism and optical properties of the columns were also discussed. Optical absorption shows that In_2O_3 columns have a high band to band transition at ∼3.75 eV. The ultraviolet and green emissions were obtained from the In_2O_3 columnar arrays. The P-N junction was formed between In_2O_3 and P-type Si substrate. The GLAD synthesized In_2O_3 film exhibits low current conduction compared to In_2O_3 TF. However, the Si/GLAD-In_2O_3 detector shows ∼1.5 times enhanced photoresponsivity than that of Si/In_2O_3 TF.

A. Mondal (✉) · B. Shougaijam · T. Goswami · J.C. Dhar · N.K. Singh
Department of Electronics and Communication Engineering, National Institute of Technology, Agartala 799055, India
e-mail: aniruddhamo@gmail.com

S. Choudhury
Department of Electronics and Communication Engineering, North Eastern Hill University, Shillong 793022, India

K.K. Chattopadhay
Department of Physics, Jadavpur University, Kolkata 700032, India

1 Introduction

Indium oxide (In_2O_3) is a wide-band gap (∼3.6 eV) [1], transparent and highly conducting [2] metal oxide semiconductor. The semiconductors having such excellent features are interesting for flexible electronics, ultraviolet (UV) detectors and sensors. Different techniques viz. dc magnetron sputtering [3], laser deposition [4], chemical vapor deposition [5], sol-gel process [6], electrochemical deposition [7] and vapor-liquid-solid (VLS) [8], etc. were employed to fabricate the one-dimensional (1D) In_2O_3 nanostructures. However, the reported nanostructures were mostly not patterned perpendicularly on the substrate. The vertically oriented and well-patterned nanostructure have a great potential to increase the photo excited electron-hole pairs and detector/solar cell efficiency by absorbing the incident photons due to multiple scattering process inside the structure as well as by channeling the carrier through the 1D structure [9]. The metal oxide nanostructures can perform good photosensitivity due to the absorption of oxygen molecules at its surface [10]. There are few reports on the synthesis of In_2O_3 nanostructures by annealing indium (In) nanoparticles (NPs), fabricated by e-beam evaporation technique [11]. Jun Tamaki et al. reported the fabrication of In_2O_3 thin film (TF) by e-beam evaporation method using In_2O_3 disc as targeted material [12]. The growth of metal oxide columns can be well controlled by a simple GLAD technique using e-beam evaporator [13]. Therefore, from the technical point of view for the development of flexible optoelectronic devices based on GLAD In_2O_3 1D structure, requires a detailed understanding of their structural and optical properties. The Si/In_2O_3 nanostructure-based devices were less studied [14]. Moreover, to our knowledge, there is no report on the heterojunction devices, fabricated by using GLAD synthesized In_2O_3 columnar structure on Si.

In this paper, we have reported the fabrication of highly ordered and perpendicular In_2O_3 columns on the ITO coated glass substrate by e-beam evaporator using the GLAD technique for the first time. The polycrystalline nature of the columns has been investigated by TEM analysis. The optical absorption measurement on the sample manifests the main band related transition in the material. The photoluminescence (PL) study was done on deposited In_2O_3 columns, to investigate the band to band and oxygen defects related sub-band gap transitions. The current conduction and photocurrent measurements were done on the Si/In_2O_3 TF as well as on the Si/GLAD-In_2O_3 devices.

2 Experimental

GLAD technique was carried out to synthesize the columnar arrays by evaporating 99.999 % pure In_2O_3 (MTI, USA) inside the chamber of e-beam evaporator (Hind High vacuum Co. (p) Ltd., 15F6) on ITO coated glass substrate (MTI, USA) at a base pressure of $\sim 2 \times 10^{-5}$ mbar. The deposition rate of 1.5 $\text{Å}\,s^{-1}$ was used to synthesize the 500 nm columnar structure, which was monitored by a quartz crystal. The substrate holder was kept at a distance of 24 cm from the evaporated material source with an azimuthal rotation of 120 rpm and an orientation of 85° with respect to the perpendicular line between the source and substrate. Seven successive depositions were carried out to synthesize the columnar film. The GLAD was also carried out to synthesize the In_2O_3 films on the P-type Si<100> substrate by applying the same experimental arrangements described above. The normal deposition of In_2O_3 (500 nm) was used to fabricate the TF devices. Indium (In) (99.999 %, MTI, USA) has been evaporated through the aluminum mask hole of diameter 1.5 mm on In_2O_3 layers to form the ohmic contact. The area of the In electrode contact was 1.77×10^{-6} m^2.

The samples were characterized by the Xrd (Bruker, D8 Advance) method using Cu Ka radiation. The FEG-SEM (JEOL, JSM-7600F) and Energy dispersive X-ray (EDX) analysis were done on the samples. The TEM (JEOL, JEM-2010) with SAED analysis has been carried out. The optical absorption measurement was done on the samples by an UV-vis near infrared spectrophotometer (Lambda 950, Perkin Elmer). The room-temperature PL study was also carried out by using xenon lamp (ELICO, SL 174) on the deposited columnar film. The current (I)-voltage (V) characteristics of the samples were investigated by using a Keithley 2400 source-measure unit from the Si/In_2O_3 TF and Si/GLAD-In_2O_3 devices. The photocurrent measurements were done under the illumination of 100 W tungsten filament bulb.

3 Results and discussions

3.1 Structural analysis

Figure 1 shows the FEG-SEM images of the sample prepared at 85° GLAD on ITO coated glass plate. The top view (Fig. 1(a)) of the sample represents some under-grown columnar region (marked by dashed circles), which can be attributed to a competitive growth mode process during the deposition [15]. The average top diameter of the column was calculated around ∼100 nm. A careful observation of FEG-SEM images showed that the columns are built of small NPs. The individual columns are interconnected to each other and form a porous oxide film, which shows sponge-like growth. This morphology has been observed for metals and oxides as a transitional structural beyond classic Zone-1 type growth [16] due to sufficient surface mobility, which can also be created under shadow growth conditions. The similar has been observed previously for GLAD processes [17] as well as in the normal incident sputter deposition [18] at high gas pressures that accentuate scattering onto the substrates to assist surface mobility, which creates interconnected regions under growth. Figure 1(b) shows the cross-sectional view of the sample, which contains the perpendicular columnar arrays. The average height of columns is ∼400 nm. The EDX spectrum (Fig. 1(c)) shows the emission from O K and In L shell. Figure 1(d) is the EDX mapping of the sample, which shows the presence of oxygen (O_2) (blue color) and indium (In) (green color).

A pull-out of a portion of the coating is seen in the TEM image of Fig. 2(a), and it can be considered as part of a loosely bonded structure with a base columnar-type spine. The morphology of the structure was examined by TEM. Figure 2(a) also shows the growth direction, which are constructed by In_2O_3 NPs. At the time of In_2O_3 deposition, these NPs act as an ideal building block for the construction of columns. The length of ∼400 nm and diameter of ∼70 nm of a typical column (Fig. 2(a)) were estimated. The melting point of In_2O_3 is ∼2000°C, but its sublimation point is not defined [19]. It has been observed that under high vacuum of 10^{-4} to 10^{-5} mbar and at the high temperatures of 1500 °C, the In_2O_3 does not show any change in weight [19]. In our case, at a chamber pressure of $\sim 2 \times 10^{-5}$ mbar and at the ambient temperature under e-beam evaporation, the In_2O_3 dissociated, sublimated and re-bound to form the small In_2O_3 NPs. The electron diffraction in SAED analysis of the column produces a pattern of concentric rings, which confirms the polycrystalline nature of the material (Fig. 2(a) inset). The high mobility of the incident atoms on the substrate under GLAD deposition produced the In_2O_3 columns which are polycrystalline in nature. Figure 2(b) shows the crystallites are randomly oriented with different spacing separated by the grain bound-

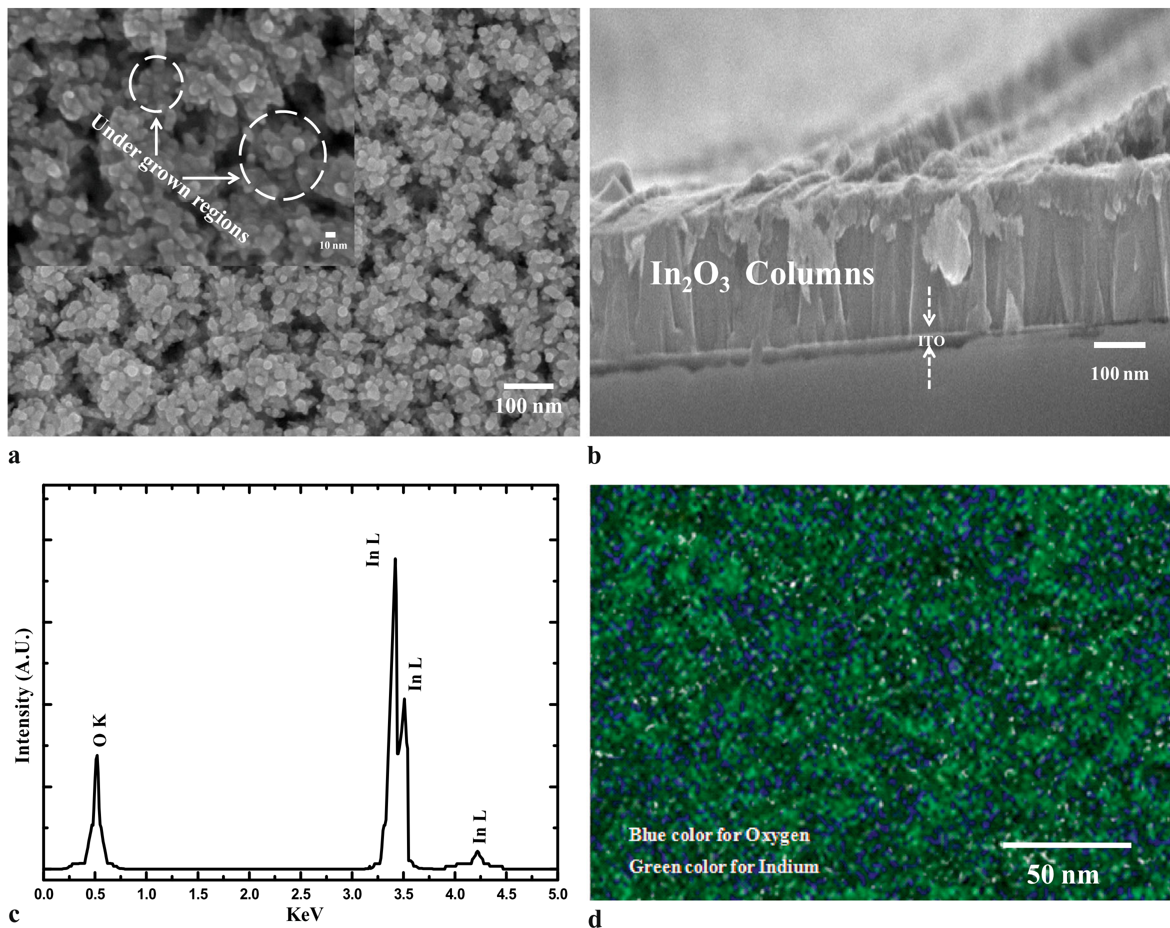

Fig. 1 FEG-SEM images of In_2O_3 columns. (**a**) Top view and under-grown columnar region (*inset*). (**b**) Cross-sectional view. (**c**) EDX spectrum. (**d**) Chemical mapping

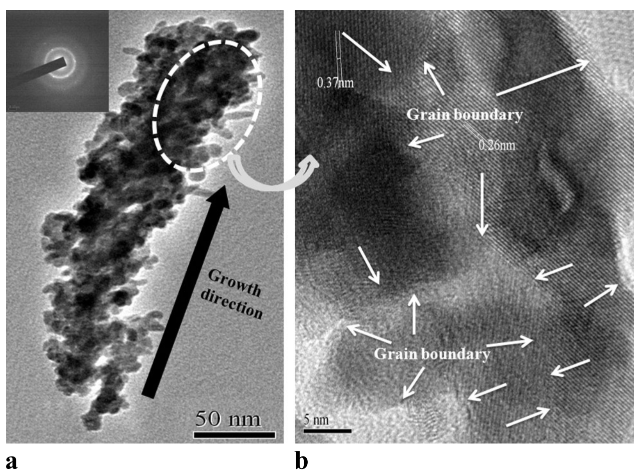

Fig. 2 TEM images (**a**) In_2O_3 column and SAED analysis (*inset*). (**b**) Randomly oriented crystallites with different spacing and grain boundaries

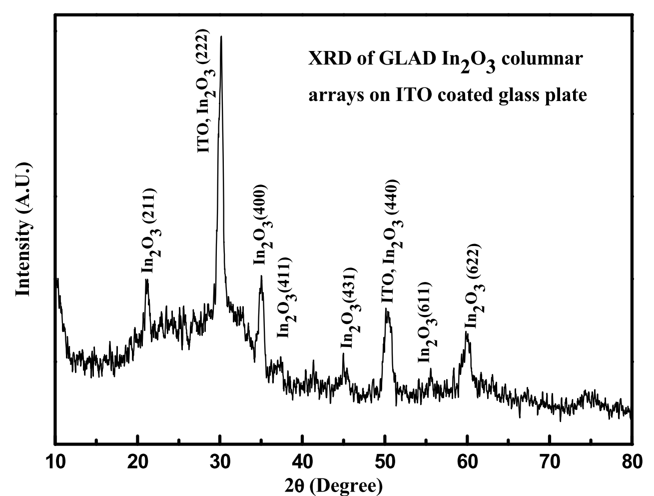

Fig. 3 XRD pattern of In_2O_3 columnar arrays on ITO coated glass plate

aries, indicated by the arrows. The spacing of 0.37 nm and 0.26 nm were measured at two distinct positions.

The XRD pattern (Fig. 3) shows the presence of different phases of the synthesized In_2O_3 columns, i.e. (211), (222),

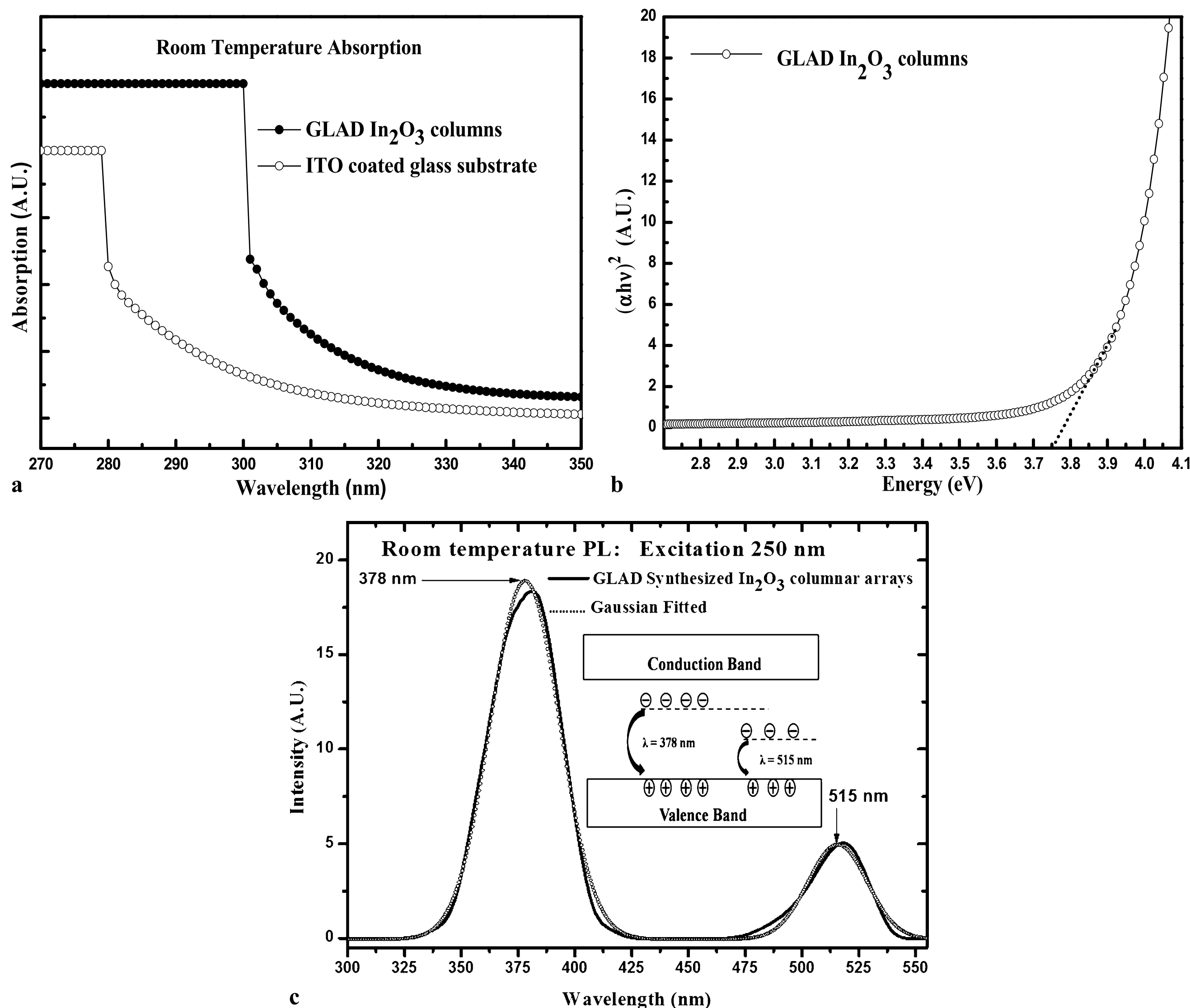

Fig. 4 UV-vis spectrum of In_2O_3 columnar arrays (**a**) absorption; (**b**) $(\alpha h\nu)^2$ versus energy curve. (**c**) Photoluminescence spectrum

(400), (411), (431), (440), (611), and (622) [JCPDS: 06-0416]. The diffraction patterns from different phases of ITO were also recognized, which were from the substrate. The XRD pattern also reveals the polycrystalline nature of the deposited In_2O_3, which support the SAED in TEM analysis.

3.2 Optical absorption and PL emission

Optical absorption measurements were done at room temperature on the as-deposited In_2O_3 columns, which has been represented together with bare ITO coated glass plate. The absorption enhancement in the UV region of the In_2O_3 columnar array is displayed in Fig. 4(a). The In_2O_3 column assembly on the ITO coated glass substrate act as an antireflection coating, which causes more scattering of the incident light on the structure and hence more absorption. The optical band gap of the fabricated columnar arrays were estimated ~3.75 eV from $(\alpha h\nu)^2$ versus $h\nu$ plot (α is the absorption coefficient, $h\nu$ is the photon energy) (Fig. 4(b)), which was greater than that of the reported value (~3.67 eV) [20] of the as-deposited In_2O_3 TF.

The room-temperature PL spectrum of In_2O_3 columnar sample was then recorded using an excitation wavelength of 250 nm. Figure 4(c) shows the PL emission from In_2O_3 columnar assembly at 378 nm (~3.3 eV, FWHM 35.8 nm) and 515 nm (~2.4 eV, FWHM 20.7 nm). However, the main band gap related transition was observed at ~3.75 eV in optical absorption, which is larger than that of the PL emission at ~3.3 eV. When a photon generates an electron-hole pair, a free exciton is formed by the Coulombic attraction, in which an electron and a hole remain bound to each other. In

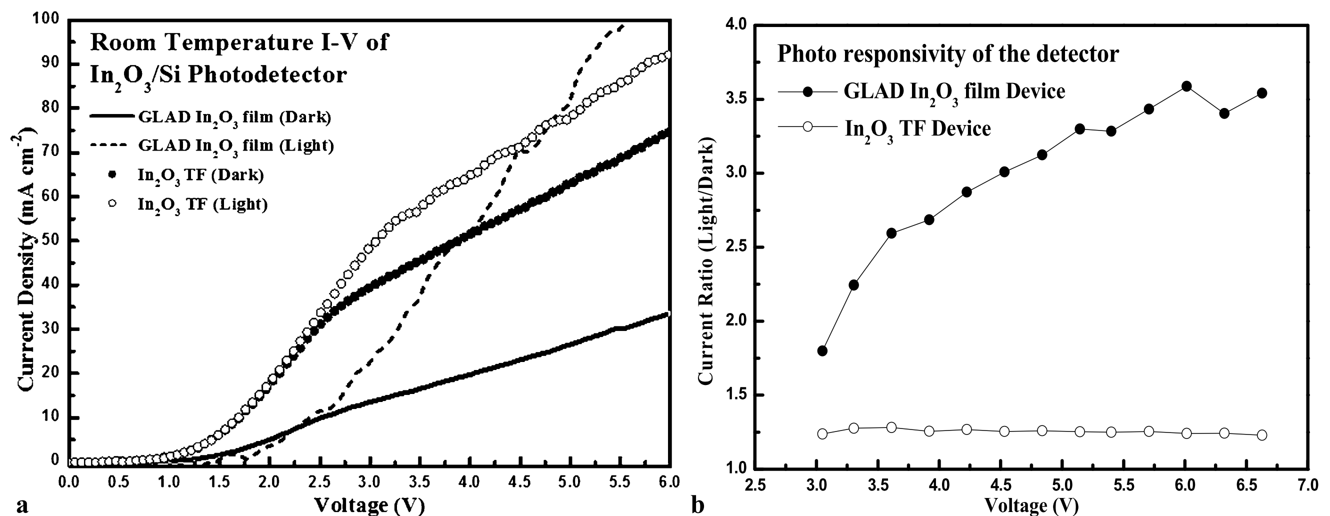

Fig. 5 (**a**) I–V characteristics of In/In_2O_3 TF/Si and In/GLAD-In_2O_3/Si under dark and light illumination. (**b**) Photosensitivity of TF and GLAD-In_2O_3 film-based detectors

the case of a free exciton related recombination process, the emitted energy is always less than the main band gap energy of the material, which is represented by the schematic band diagram (Fig. 4(c) (inset)). The low energy PL emission at ~3.3 eV may be due to the free exciton related recombination process, which can be attributed as near band gap transition. Again, the oxygen vacancy induced donor levels, which was formed in the midst of the In_2O_3 band gap [6]. It is already reported that the emission at ~514 nm is due to the oxygen vacancy created in In_2O_3 [8]. Therefore, in our case, the observed emission at 515 nm (~2.4 eV) must be from the electron-hole recombination between the valence band and the oxygen donor level. Finally, we have observed the UV light emission (~378 nm) as well as green light emission (~515 nm) from the In_2O_3 columnar assembly.

3.3 Si/In_2O_3 detector and photodetection

The devices were fabricated on P-type Si⟨100⟩ substrate of 1–30 Ω cm. Figure 5(a) shows the I–V characteristics (dark current) for Si/In_2O_3 TF and Si/GLAD-In_2O_3 devices through In ohmic contact. The current for all structure shows the rectifying behavior, which may be due to the formation of P–N junction at the interface of P-type Si and N-type In_2O_3 layer. Under the forward bias condition, the In_2O_3 TF-based detector (turn on voltage 1.3 V) shows higher current conduction behavior than that of GLAD-In_2O_3 film-based device (turn on voltage 1.5 V). The surface defects can produce surface states within the band gap making the GLAD-In_2O_3 behave like a weakly conductive material, which also observed for other metal oxide semiconductor like TiO_2 [21]. In case of GLAD-In_2O_3 film, there is a higher surface defect (due to high surface stress [22]), which allows more scattering of the electrons inside the GLAD-In_2O_3 structure and hence makes weaker conducting material than In_2O_3 TF. From Fig. 5(a), the dark currents of In_2O_3 TF and GLAD-In_2O_3 film-based devices were exerted to be 51 mA/cm^2 and 20 mA/cm^2 at 4 V, which increased to 64 mA/cm^2 and 51 mA/cm^2, respectively, under the illumination of 100 W filament bulb from a vertical distance of 12 cm from the devices. The increased responsivity was due to the decrease in the barrier height at the Si/In_2O_3 heterojunction under light illumination, which causes more carriers to get across the barrier and therefore, enlarges the current [23]. The photoresponsivity of the devices were then calculated for the forward bias condition from the ratio of light to dark current of the Si/GLAD-In_2O_3 and Si/In_2O_3 TF detector separately. An averagely 1.5 fold enhanced photosensitivity of the Si/GLAD-In_2O_3 device was observed compared to that of Si/In_2O_3 TF under the applied potential range of 3 to 6.75 V, shown in Fig. 5(b). It has been demonstrated that metal oxide nanostructures like ZnO adsorb oxygen molecules at the surface and capture free electrons so that a low-conductive depletion layer is formed near the surface [24]. Under light illumination with a photon energy larger than the semiconductor bandgap, electron-hole pairs are generated. The generated holes then quickly appear at the nanostructure surface and discharge the negatively charged adsorbed oxygen ions, leaving behind unpaired electrons. Thus, band bending occurs and the conductivity of the nanostructure increases. In the present situation, the GLAD-In_2O_3 film has high density of trap states (usually found in nanostructure) due to the dangling bonds at the surface than that of In_2O_3 TF, which enhance the absorption of oxygen molecules at the GLAD-In_2O_3 surface and thus the photoresponse. Also, the GLAD-In_2O_3 nanostructure consists of a large amount of atoms per unit volume

at the surface [25], which creates more electron-hole pairs under photon excitation than that of the TF and therefore, responsible for high photosensitivity.

4 Conclusion

In this work, a template-free atomic shadow assisted GLAD method was introduced for the preparation of perpendicular In_2O_3 columns on the ITO coated glass plate. The polycrystalline nature of the In_2O_3 was obtained due to high mobility of the incident atom on the substrate and shows a high band gap at ∼3.75 eV and near band gap PL emission in the ultraviolet region. The green emission was due to the free exciton related recombination process in the material. This method can be developed to prepare several metal oxides columnar structure for the application of optoelectronic devices. The GLAD-In_2O_3 film has the higher surface defects, which decreases electron mobility through scattering. Large dangling bonds at the surface of GLAD-In_2O_3 film absorb oxygen molecules, produces low-conductive depletion layer at its surface, which may be the reason of less conductive compared to In_2O_3 TF. Averagely 1.5 fold enhanced photoresponsivity (bias voltage 3–6.75 V) was observed from Si/GLAD-In_2O_3 compared to Si/In_2O_3 TF detector, due to more electron-hole pairs generated in GLAD-In_2O_3 film.

Acknowledgements The authors are thankful to Dr. Ardhendu Saha of Electrical Engineering Department, NIT Agartala for the optical measurement, Dr. Syed A. Hussain of physics department, Tripura university for providing I-V measurement and SAIF, IIT Bombay, India for FEG-SEM measurement and also Department of Science and Technology, India for financial support.

References

1. M. Amith, A. Barve, V.J. Leppert, Nano Lett. **1**, 287 (2001)
2. O. Bierwagen, J.S. Speck, Appl. Phys. Lett. **97**, 072103 (2010)
3. B.R. Krishna, T.K. Subramanyam, B.S. Naidu, S. Uthanna, Opt. Mater. **15**, 217 (2000)
4. F. Liu, M. Bao, K.L. Wang, C. Li, B. Lei, C. Zhou, Appl. Phys. Lett. **86**, 213101 (2005)
5. G. Cheng, E. Stern, S. Guthrie, M.A. Reed, R. Klie, Y. Hao, G. Meng, L. Zhang, Appl. Phys. A **85**, 233 (2006)
6. H. Cao, X. Qiu, Y. Liang, Q. Zhu, M. Zhao, Appl. Phys. Lett. **83**, 761 (2003)
7. M.J. Zheng, L.D. Zhang, G.H. Li, X.Y. Zhang, X.F. Wang, Appl. Phys. Lett. **79**, 839 (2001)
8. T.S. Ko, C.P. Chu, J.R. Chen, T.C. Lu, H.C. Kuo, S.C. Wang, J. Cryst. Growth **310**, 2264 (2008)
9. P. Chinnamuthu, J.C. Dhar, A. Mondal, A. Bhattacharyya, N.K. Singh, J. Phys. D, Appl. Phys. **45**, 135102 (2012)
10. W. Park, G. Jo, W.K. Hong, J. Yoon, M. Choe, Nanotechnology **22**, 205204 (2011)
11. R. Winter, K. Scharnagl, A. Fuchs, T. Doll, I. Eisele, Sens. Actuators B **66**, 85 (2000)
12. J. Tamaki, C. Naruo, Y. Yamamoto, M. Matsuoka, Sens. Actuators B **83**, 190 (2002)
13. K. Robbie, G. Beydaghyan, T. Brown, C. Dean, J. Adams, C. Buzea, Rev. Sci. Instrum. **75**, 1089 (2004)
14. R.A. Ismail, D.N. Raouf, D.F. Raouf, J. Optoelectron. Adv. Mater. **8**, 1443 (2006)
15. C.M. Zhou, D. Gall, Appl. Phys. Lett. **90**, 093103 (2007)
16. S. Mahieu, P. Ghekiere, D. Depla, R.D. Gryse, Thin Solid Films **515**, 1229 (2006)
17. S. Mukherjee, D. Gall, Thin Solid Films **527**, 158 (2013)
18. T. Karabacak, J.J. Senkevich, G.C. Wang, T.M. Lu, J. Vac. Sci. Technol. A **24**, 986 (2005)
19. E. Ishii, M. Nakane, H. Ishikawa, I. Uehara, Y. Miyake, United States Patent US 4202917, 13 May 1980
20. V. Senthilkumar, P. Vickraman, Curr. Appl. Phys. **10**, 880 (2010)
21. X. Lin, X.B. He, T.Z. Yang, W. Guo, D.X. Shi, H.J. Gao, D.D.D. Ma, S.T. Lee, F. Liu, X.C. Xie, Appl. Phys. Lett. **89**, 043103 (2006)
22. F. Song, G.L. Huang, H.S. Park, X.N. Liu, Int. J. Solids Struct. **48**, 2154 (2011)
23. N. Vanhove, J. John, A. Lorenz, K. Cheng, G. Borghs, J.E.M. Haverkort, Appl. Surf. Sci. **253**, 2930 (2006)
24. S.N. Das, K.J. Moon, J.P. Kar, J.H. Choi, J. Xiong, Appl. Phys. Lett. **97**, 022103 (2010)
25. D. Vanmaekelbergh, L.V. Pieterson, Phys. Rev. Lett. **80**, 821 (1998)